Size-Dependent Intrinsic Radiative Decay Rates of Silicon Nanocrystals at Large Confinement Energies

Milan Sykora,[1] Lorenzo Mangolini,[2] Richard D. Schaller,[1] Uwe Kortshagen,[2] David Jurbergs,[3] and Victor I. Klimov[1]

[1]*Chemistry Division, Los Alamos National Laboratory, MS-J567, Los Alamos, New Mexico 87545, USA*

[2]*Department of Mechanical Engineering, High Temperature and Plasma Laboratory, University of Minnesota, Minneapolis, Minnesota 55455, USA*

[3]*Innovalight Inc., 3303 Octavius Drive, Suite 104, Santa Clara, California 95054, USA*

(Received 6 July 2007; published 14 February 2008)

We study ultrafast photoluminescence (PL) dynamics of Si nanocrystals (NCs). The early-time PL spectra (<1 ns), which show strong dependence on NC size, are attributed to emission involving NC quantized states. The PL spectra recorded for long delays (> 10 ns) are almost independent of NC size and are likely due to surface-related recombination. Based on instantaneous PL intensities measured 2 ps after excitation, we determine intrinsic radiative rate constants for NCs of different sizes. These constants sharply increase for confinement energies greater than ~1 eV indicating a fast, exponential growth of the oscillator strength of zero-phonon, pseudodirect transitions.

DOI: 10.1103/PhysRevLett.100.067401 PACS numbers: 78.67.−n, 71.35.−y, 78.47.−p, 78.55.−m

Bulk Si is an indirect-gap semiconductor, and thus, the radiative recombination in this material can occur only via low-efficiency, phonon-assisted processes. Following the initial observation of efficient photoluminescence (PL) from porous Si [1,2], there have been numerous reports on greatly enhanced emission efficiencies in various types of Si nanostructures [3–6]. For example, a recently developed plasma-synthesis and organic surface passivation technique produces Si nanocrystals (NCs) with a PL quantum yield >60% [7]. The mechanism for high-efficiency PL from Si nanostructures is still under debate [5,6]. For example, ''surface-state'' models ascribe it to recombination of carriers trapped at surface sites [8], while ''quantum-confinement'' models explain it by recombination across the fundamental nanostructure band gap. In the latter case, the increase in the radiative rate is attributed to confinement-induced relaxation of momentum conservation, which opens an additional radiative decay channel via zero-phonon, *pseudodirect* transitions.

In this Letter, we analyze the evolution of PL spectra of Si NCs on subpicosecond to submicrosecond time scales using different spectroscopic techniques. This analysis allows us to distinguish between contributions from intrinsic NC-core and extrinsic (likely surface-related) states. The core-state emission dominates early-time PL spectra that show strong dependence on NC size. The spectrum of late-time emission (>10 ns) does not vary significantly with NC size, which is a signature of surface-related recombination [9,10]. On the basis of emission rates measured immediately after excitation, we infer that the intrinsic radiative rate constants exhibit fast, exponential growth for confinement energies greater than ~1 eV, which indicates a rapid increase in the strength of zero-phonon transitions.

We have studied Si NCs fabricated by two different methods: laser-induced SiH_4 pyrolysis [11,12] (series-A samples) and room-temperature plasma dissociation of SiH_4 [7,13] (series-B samples). For both methods, the mean NC diameter was smaller than 4 nm and the NC-size distribution had a standard deviation of 15%–20%. Electron microscopy and x-ray diffraction studies indicate a high degree of crystallinity of the NCs. The NC surfaces were functionalized with 1-octadecence (series A) or 1-dodecene (series B) [7] in order to passivate surface traps and to make NCs soluble. Spectroscopic studies were conducted at room temperature using NC hexane solutions; a cell with NCs was continuously moved during the measurements to avoid sample degradation.

The NCs were studied by steady-state PL (SSPL) and two different time-resolved PL methods. The PL dynamics in the nanosecond regime were monitored with 70 ps time resolution using a time-correlated single photon counting (TCSPC) system (excitation by 3.1 eV, 50 ps pulses from a pulsed diode laser). Femtosecond PL measurements (300 fs time resolution) were performed using PL up-conversion (UPL) [14], in which the emission from a sample excited by 3.1 eV, 200 fs pulses at 250 kHz (frequency-doubled amplified Ti:sapphire laser) was frequency-mixed (gated) with 1.55 eV, 200 fs pulses in a nonlinear-optical crystal.

Figure 1(a) shows SSPL and early-time ($t = 2$ ps) UPL spectra of a series-A sample. The UPL band is blue-shifted by 0.32 eV with respect to the SSPL band. Other *A*- and *B*-type samples exhibit a similar shift with the magnitude, which increases for samples emitting at lower energies [Fig. 1(b)]. An analogous shift between the steady-state and early-time PL was recently reported for Si NCs embedded in a sol-gel SiO_2 matrix [15].

In Fig. 2(a), we show steady-state and time-resolved PL spectra (TCSPC) of a series-B sample. On short time scales (<1 ns), the emission is dominated by a high-energy band (~2.3 eV), shifted from the SSPL maximum by

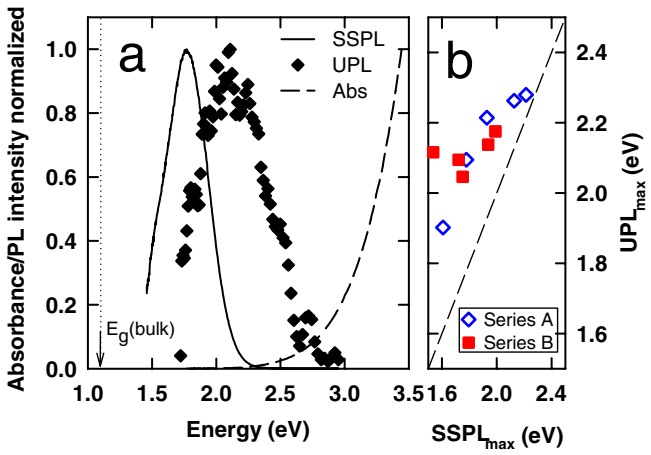

FIG. 1 (color online). (a) SSPL (solid lines), UPL (symbols; $t = 2$ ps, pump fluence $j_p = 0.5$ mJ cm^{-2}), and absorption (dashed line) spectra for a series-A Si NC sample. The arrow marks the energy gap of bulk Si. (b) The UPL spectral maximum versus the SSPL maximum for all of the series-A and series-B samples studied here (symbols); the dashed line corresponds to the situation where UPL and SSPL have the same emission maxima.

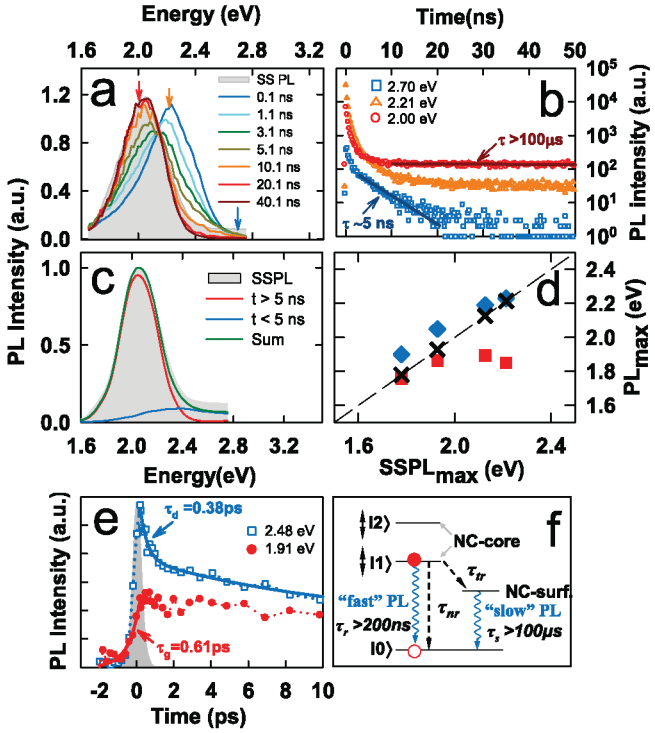

FIG. 2 (color). (a) Time-resolved PL (lines; TCSPC, $j_p = 0.38$ μJ cm^{-2}) and SSPL (gray shading) spectra of Si NCs (series-B sample); the TCSPC spectra are normalized to the same area. (b) Time transients (symbols) measured for three spectral energies indicated by arrows in panel (a); lines are single-exponential fits. (c) The PL spectra of a series-A sample generated by integrating spectrally resolved PL dynamics for time intervals $t = 0$–5 ns (blue line) and $t > 5$ ns (red line) and the sum spectrum (green line) in comparison to the measured SSPL (gray shading). (d) The dependence of the maxima of the short-lived (blue diamonds) and the long-lived (red squares) PL bands on the SSPL maximum (shown also along the vertical axes by crosses). (e) Early-time PL dynamics for a series-A sample monitored at 1.91 eV (solid circles) and 2.48 eV (open squares). The signal buildup at the lower energy ($\tau_b = 0.61$ ps) is complimentary to the hot PL decay at the higher energy ($\tau_d = 0.38$ ps). (f) Schematics of relaxation processes in Si NCs. Following photoexcitation, an exciton relaxes into the lowest energy quantized state, $|1\rangle$, from which it can either recombine radiatively ("fast," high-energy PL feature, τ_r) or nonradiatively (τ_{nr}) or get trapped at the surface (τ_{tr}) and then recombine through the surface site ("slow," low-energy PL feature, τ_s). Energies of the NC-core states are size dependent, while the energy of the surface state is virtually NC-size independent.

~300 meV [consistent with UPL results in Fig. 1(a)]. On longer time scales, we observe a gradual shift of the PL maximum to the red until it eventually reaches the SSPL maximum (~2 eV). The temporal evolution of the PL indicates the existence of two emitting states that are responsible for early-time (high-energy state) and late-time (low-energy state) emission. The fact that only two species contribute to PL is also supported by the appearance of an isostilbic point [at ~2.2 eV in Fig. 2(a)] in time-resolved PL spectra normalized to the same area [16,17]. Each of the emitting states is likely distributed in energy (because of sample polydispersity); however, these distributions are characterized by distinct central energies [~2.3 eV and 2.05 eV in Fig. 2(a)] and time-independent line shapes [16].

The existence of two distinct emission sources is also evident from the PL dynamics in Fig. 2(b) that indicate two distinct relaxation time scales. The PL relaxation at high spectral energies is dominated by fast, ~5 ns decay, while on the low-energy side, this fast component is superimposed on a large, slow background with a decay constant of >100 μs. Similar PL dynamics with two different time scales are also observed for series-A samples and were recently reported in Ref. [18] for ion-implanted Si NCs.

To spectrally map the states responsible for the fast and the slow PL decay, we integrate spectrally resolved transients for time intervals $t = 0$–5 ns and $t > 5$ ns. This procedure shows that the fast PL decay component originates from higher-energy states [blue line in Fig. 2(c)], while the slow-decaying background is due to lower-energy states [red line in Fig. 2(c)]. The superposition of the slow and fast spectra [green line in Fig. 2(c)] closely reproduces the SSPL spectrum (gray shading). Further, we observe that for this particular sample, the SSPL is dominated by the low-energy state, while the high-energy state contributes only a weak high-energy shoulder to the spectrum. A similar analysis applied to other samples shows that the high-energy feature becomes progressively more important for smaller NCs. We also observe that this band plays a major role in defining the size dependence of the

SSPL. As evident from Fig. 2(d), the spectral maxima of the fast component tracks the changes in the position of the SSPL maximum, while the position of the slow component is almost independent of NC size.

The pronounced high-energy shift of the fast PL band for smaller NCs indicates that it is likely due to NC-core emission, which is expected to be strongly affected by quantum confinement. Further, the fast buildup of this band [$\tau_b = 0.61$ ps; Fig. 2(e), solid circles] suggests that it develops before processes such as surface trapping can occur; hence, it cannot be due to surface defects. Finally, this band cannot be attributed to "hot" carrier emission. The latter is observed as a high-energy shoulder in early-time spectra and is characterized by extremely short, ~0.38 ps decay [Fig. 2(e); squares], which indicates large intraband relaxation rates, comparable to those in, e.g., CdSe NCs [19].

The low-energy, slow band, which does not show significant size dependence is likely to be surface related and, as suggested in Refs. [9,10], may be due to a recombination of an electron-hole pair, in which one or both carriers are localized on a surface bond. This low-energy state is possibly populated as a result of relaxation of carriers from the higher-energy NC-core states. In the latter scenario, the 5 ns time constant measured for the high-energy band determines the time scale of such a relaxation process [Fig. 2(f)].

Because of potentially significant nonradiative losses, the dynamics measured for the high-energy band cannot be used to infer the radiative decay time (τ_r) of quantized states. Therefore, here we determine τ_r by analyzing instantaneous emission rates (r_e) that are measured by integrating time-resolved UPL spectra. The value of r_e is proportional to the radiative recombination rate, n/τ_r (n is the concentration of emitters), and, hence, τ_r can be determined by comparing the spectrally integrated UPL intensity for a Si NC sample (I) with that of a reference sample (I^R) with a known radiative rate. We perform UPL measurements immediately after excitation ($t = 2$ ps) to ensure that the number of emitting NCs is determined by the number of absorbed photons. The latter is proportional to the product of the absorption coefficient (α_0) and the pump fluence (j_p), and, hence, $\tau_r = \tau_r{}^R(\alpha_0/\alpha_0{}^R) \times (j_p/j_p{}^R)(I/I^R)$, where superscript R denotes values for the reference sample.

In the inset of Fig. 3(a), we show UPL spectra for several Si NC samples with different emission wavelengths (lines) together with the UPL spectrum of a reference CdSe NC sample (gray shading; $\tau_r = 20$ ns [22]). One obvious trend in these data is a rapid increase in the UPL intensity of Si NCs with increasing emission energy, which indicates an increase in the radiative rate constant ($k_r = 1/\tau_r$) for smaller NCs. The values of k_r derived from the UPL spectra are shown in Fig. 3 versus the UPL emission maximum ($\hbar\omega_m$). We observe that radiative decay is relatively slow for larger particles with $\hbar\omega_m < 2$ eV [e.g., $k_r \approx 0.13\ \mu s^{-1}$ ($\tau_r \approx 8\ \mu s$) for $\hbar\omega_m = 1.9$ eV]. However, k_r sharply increases for particles of smaller sizes (higher emission energy); for example, $k_r \approx 5\ \mu s^{-1}$ ($\tau_r \approx 200$ ns) for NCs with $\hbar\omega_m = 2.3$ eV. This growth explains the increase in the contribution from the NC-core emission to the SSPL for smaller NC sizes, which results in the convergence of the SSPL and the UPL band positions at large confinement energies [Fig. 1(b)].

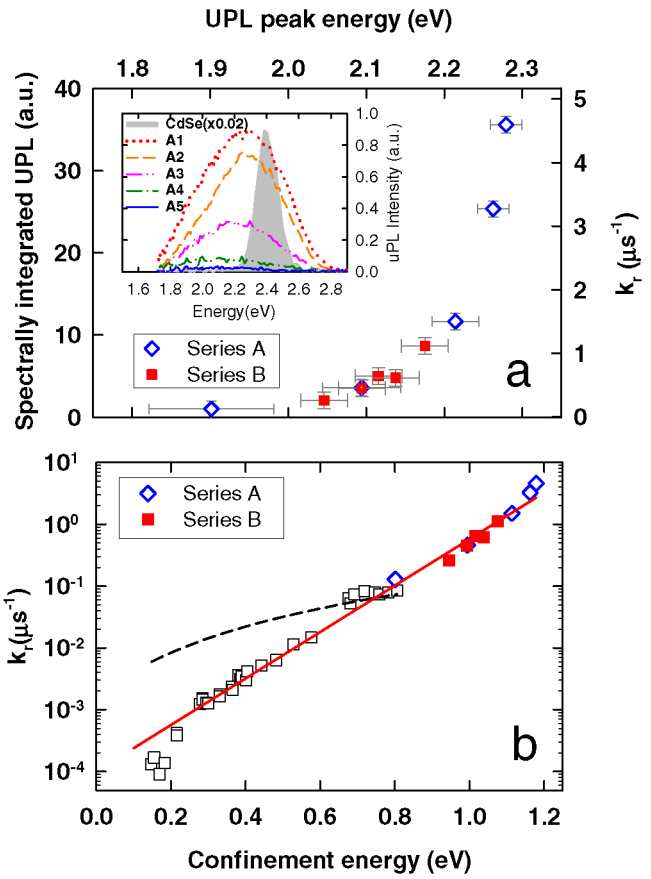

FIG. 3 (color online). (a) The radiative rate constant versus the UPL peak position for series-A (diamonds) and series-B (squares) Si NC samples. These data were derived from spectrally integrated UPL spectra measured at 2 ps for Si NCs (lines in the inset; series-A samples) and the reference CdSe NC sample (gray shading in the inset). All samples had approximately the same optical density at the pump wavelength and were excited with the same pump fluences. (b) The dependence of the radiative rate constant on the NC confinement energy (solid squares and open diamonds; this work) in comparison to pseudodirect transition rates derived from the experimental data of Ref. [20] (open squares) and calculated phonon-assisted decay rates (dashed line) from Ref. [21]. The rates of pseudodirect recombination can be closely described by an exponential dependence (solid line).

The findings described above are consistent with a NC-core origin of the high-energy, fast PL band. In addition to

increasing the energy gap, quantum confinement is expected to mix states with different k vectors [21,23,24], which opens an additional radiative decay channel via zero-phonon, pseudodirect transitions. A theoretical analysis of Ref. [21] shows that this effect becomes significant for confinement energies (E_c) of $\sim$1 eV (emission energy of $\sim$2.1 eV), when the rates of the indirect and pseudodirect recombination become comparable. The latter conclusion is consistent with previous experimental studies of relative intensities of the zero-phonon and the phonon-assisted PL features [20]. Since the strength of pseudodirect transitions increases with decreasing NC size much faster than the strength of indirect transitions [20,21], the total recombination rate is expected to rapidly grow for E_c greater than 1 eV, which is exactly the trend observed in our experiments.

There is also a reasonable agreement between absolute values of the calculated decay rates with those measured by us for low confinement energies, for which radiative recombination is presumably still primarily indirect. For example, for $E_c = 0.8$ eV, we measure $k_r \approx 0.13\ \mu s^{-1}$, while the calculated total rate is $\sim 0.1\ \mu s^{-1}$ [20,21]. On the other hand, in the range of large E_c, for which radiative decay is anticipated to be dominated by pseudodirect transitions, the measured values of k_r show a much faster growth with E_c than predicted theoretically. Within the effective-mass model, the rate constant of the zero-phonon transitions shows scaling $k_r \propto (E_c)^{6/X}$, where $1.2 \leq X \leq 2$, depending on the NC-size dependence of E_c. On the other hand, our measurements indicate a fast exponential growth: $k_r \propto \exp(E_c/E_0)$ with $E_0 = 115$ meV [Fig. 3(b), solid line].

Interestingly, the same exponential dependence describes well the rate constants for smaller confinement energies calculated by multiplying the ratio of the strengths of the direct and indirect transitions measured in Ref. [20] by the theoretical rate of the phonon-assisted transitions from Ref. [21]. The data produced by this procedure [open squares in Fig. 3(b)] lie close to the exponential dependence derived from our measurements for larger E_c. The observed correspondence between the two data sets is particularly remarkable given that they span a wide range of confinement energies ($\sim$0.4–1.2 eV) and 4 orders of magnitude in the transition rate. It is also noteworthy that these data are consistent for samples produced by four different methods (two different gas phase techniques in our work and electrochemical etching and high-temperature precipitation in SiO_2 in Ref. [20]). This strongly suggests that the observed rapid increase in the rate of zero-phonon recombination with E_c is not sample-dependent, but is intrinsic to Si NCs.

In conclusion, the analysis of time-resolved PL from Si NCs suggests the existence of two sources of emission with distinct spectral and dynamical properties that we attribute to intrinsic NC-core states (high-energy, fast PL feature) and extrinsic, likely surface-related states (low-energy, slow feature). Using instantaneous emission rates measured shortly after excitation, we derive radiative decay rates for quantum-confined NC states. These rates show fast exponential growth with confinement energy for emission energy >2 eV, which indicates a rapid increase in the efficiency of pseudodirect recombination.

This work was supported by the Office of Basic Energy Sciences, U.S. Department of Energy (DOE), Los Alamos LDRD funds, and the DOE Center for Integrated Nanotechnologies. L. M. and U. K. were supported by NSF and in part by MRSEC grants.

[1] L. T. Canham, Appl. Phys. Lett. **57**, 1046 (1990).
[2] V. Lehmann and U. Gosele, Appl. Phys. Lett. **58**, 856 (1991).
[3] P. M. Fauchet and L. Tsybeskov, Proc. SPIE-Int. Soc. Opt. Eng. **3283**, 793 (1998).
[4] D. Kovalev *et al.*, Phys. Status Solidi B **215**, 871 (1999).
[5] A. G. Cullis, L. T. Canham, and P. D. J. Calcott, J. Appl. Phys. **82**, 909 (1997).
[6] P. M. Fauchet, J. Lumin. **70**, 294 (1996).
[7] D. Jurbergs *et al.*, Appl. Phys. Lett. **88**, 233116 (2006).
[8] F. Koch and V. Petrova-Koch, J. Non-Cryst. Solids **198/200**, 840 (1996).
[9] G. Allan, C. Delerue, and M. Lannoo, Phys. Rev. Lett. **76**, 2961 (1996).
[10] M. V. Wolkin *et al.*, Phys. Rev. Lett. **82**, 197 (1999).
[11] X. G. Li *et al.*, Langmuir **19**, 8490 (2003).
[12] X. G. Li, Y. Q. He, and M. T. Swihart, Langmuir **20**, 4720 (2004).
[13] L. Mangolini, E. Thimsen, and U. Kortshagen, Nano Lett. **5**, 655 (2005).
[14] J. Shah, IEEE J. Quantum Electron. **24**, 276 (1988).
[15] F. Trojanek *et al.*, J. Appl. Phys. **99**, 116108 (2006).
[16] If PL is contributed by more than two species, the appearance of the isostilbic point is unlikely, because it would require that the area-normalized spectral profiles of all of the species intersect at a single point. See EPAPS Document No. E-PRLTAO-100-074804 for the detailed analysis of conditions required for the observation of the isostillbic point. For more information on EPAPS, see http://www.aip.org/pubservs/epaps.html.
[17] A. S. R. Koti, M. M. G. Krishna, and N. Periasamy, J. Phys. Chem. A **105**, 1767 (2001).
[18] F. Trojanek *et al.*, Phys. Rev. B **72**, 075365 (2005).
[19] V. I. Klimov and D. W. McBranch, Phys. Rev. Lett. **80**, 4028 (1998).
[20] D. Kovalev *et al.*, Phys. Rev. Lett. **81**, 2803 (1998).
[21] M. S. Hybertsen, Phys. Rev. Lett. **72**, 1514 (1994).
[22] S. A. Crooker *et al.*, Appl. Phys. Lett. **82**, 2793 (2003).
[23] N. A. Hill and K. B. Whaley, Phys. Rev. Lett. **75**, 1130 (1995).
[24] C. Delerue, G. Allan, and M. Lannoo, Phys. Rev. B **48**, 11 024 (1993).